New Phytologist

Research

Methods

The bias of a two-dimensional view: comparing two-dimensional and three-dimensional mesophyll surface area estimates using noninvasive imaging

Guillaume Théroux-Rancourt[1]*, J. Mason Earles[2]*, Matthew E. Gilbert[1], Maciej A. Zwieniecki[1], C. Kevin Boyce[3], Andrew J. McElrone[4,5] and Craig R. Brodersen[2]

[1]Department of Plant Sciences, University of California Davis, Davis, CA 95616, USA; [2]School of Forestry & Environmental Studies, Yale University, New Haven, CT 06511, USA; [3]Department of Geological Sciences, Stanford University, Stanford, CA 94305, USA; [4]USDA-Agricultural Research Service, Davis, CA 95616, USA; [5]Deparment of Viticulture and Enology, University of California, Davis, CA 95616, USA

Author for correspondence:
Guillaume Théroux-Rancourt
Tel: +1 530 752 1703
Email: gtrancourt@ucdavis.edu

Received: *5 April 2017*
Accepted: *5 June 2017*

New Phytologist (2017)
doi: 10.1111/nph.14687

Key words: biodiversity, CAM plants, high resolution X-ray microcomputed tomography (microCT), leaf anatomy, leaf functional traits, mesophyll.

Summary

- The mesophyll surface area exposed to intercellular air space per leaf area (S_m) is closely associated with CO_2 diffusion and photosynthetic rates. S_m is typically estimated from two-dimensional (2D) leaf sections and corrected for the three-dimensional (3D) geometry of mesophyll cells, leading to potential differences between the estimated and actual cell surface area.
- Here, we examined how 2D methods used for estimating S_m compare with 3D values obtained from high-resolution X-ray microcomputed tomography (microCT) for 23 plant species, with broad phylogenetic and anatomical coverage.
- Relative to 3D, uncorrected 2D S_m estimates were, on average, 15–30% lower. Two of the four 2D S_m methods typically fell within 10% of 3D values. For most species, only a few 2D slices were needed to accurately estimate S_m within 10% of the whole leaf sample median. However, leaves with reticulate vein networks required more sections because of a more heterogeneous vein coverage across slices.
- These results provide the first comparison of the accuracy of 2D methods in estimating the complex 3D geometry of internal leaf surfaces. Because microCT is not readily available, we provide guidance for using standard light microscopy techniques, as well as recommending standardization of reporting S_m values.

Introduction

Leaf photosynthetic function is directly linked to tissue-level anatomy which can be grossly categorized into vascular, mesophyll, and epidermal cell types. Chloroplasts predominantly inhabit mesophyll cells in most vascular plants and require access to sufficiently high [CO_2] to maximize net assimilation. Consequently, terrestrial plants have evolved leaves that facilitate intercellular CO_2 diffusion, such as amphistomatal leaves (e.g. Parkhurst & Mott, 1990) and extensive contiguous air spaces to promote lateral diffusion (Pieruschka *et al.*, 2006; Morison *et al.*, 2007). Moreover, chloroplasts are typically positioned within mesophyll cells immediately adjacent to the intercellular air space (IAS) to minimize the liquid CO_2 diffusion path length (e.g. Evans *et al.*, 2009; Tholen & Zhu, 2011). For these reasons, mesophyll cell surface area per leaf area (S_m) is positively related to CO_2 diffusion and maximum leaf photosynthetic capacity (A_{max}; Nobel, 1977).

S_m is therefore a functionally important trait to measure when comparing genotypes and phenotypes (e.g. Tholen *et al.*, 2008; Giuliani *et al.*, 2013) and when comparing growth responses to environmental factors. As one example, exposure to high light intensity during development tends to result in thicker leaves with a greater proportion of palisade cells, leading to a greater S_m with higher photosynthetic capacity for a given species (e.g. Nobel, 1976; Terashima *et al.*, 2006). This correlation between S_m and A_{max} is observed for a number of species (Nobel, 1977; Longstreth *et al.*, 1980; Tosens *et al.*, 2012; Chatelet *et al.*, 2013), although other geometric constraints, such as cell wall thickness (e.g. Tosens *et al.*, 2016) and the coverage of mesophyll cell surface by chloroplasts (S_c, surface of chloroplast exposed to the IAS; e.g. Tholen *et al.*, 2008), will ultimately limit how much S_m can increase A_{max}.

Numerous methods have been developed for estimating mesophyll surface area, all of which are derived from two-dimensional

*These authors contributed equally to this work.

(2D) leaf sections and employ a means of correcting the 2D data to estimate the three-dimensional (3D) geometry. Specifically, we found five unique methods in the literature to convert 2D measurements into 3D S_m values: paradermal + cross-section (Turrell, 1936); cells as regular geometrical objects (Nobel *et al.*, 1975; Sack *et al.*, 2013); curvature correction (Thain, 1983); oblique paradermal section (James *et al.*, 1999); and stereological methods (Chabot & Chabot, 1977; Parkhurst, 1982; Kubínová, 1994; Ivanova & P'yankov, 2002). The regular geometrical objects method assumes that each cell's entire surface is exposed to the IAS, whereas other methods either are not specific (curvature correction, stereological methods such as the fakir grid method of Kubínová, 1994) or measure only the surface exposed to the IAS (Turrell, 1936; Evans *et al.*, 1994; James *et al.*, 1999). The stereological methods, using counts of intersection between the cell surface and sampling lines, make fewer assumptions regarding cell shape to infer 3D areas from 2D cross-sections (Parkhurst, 1982). However, stereological methods assume a randomly distributed spatial structure and, as a result, such methods may not be appropriate for leaves that are both anisotropic and nonrandom (Ivanova & P'yankov, 2002) and have been less commonly adopted.

Estimates of S_m from 2D cross-sections, regardless of the method, are necessarily approximations of the true 3D geometry of the internal leaf surfaces. To date, these methods have not been validated because of the difficulty in obtaining surface area measurements of such complex cellular shapes with a nonuniform arrangement. As efforts to improve crop performance could one day focus on mesophyll traits (Zhu *et al.*, 2010; Evans, 2013), it is critical to develop a better understanding of the inherent flaws or inaccuracies related to traditional 2D methods. Resolving these uncertainties will allow for further refinement of the relationship between leaf internal surface area and photosynthetic function.

Here, we compare four of the five 2D S_m estimation methods mentioned earlier with 3D values obtained using noninvasive high-resolution X-ray microcomputed tomography imaging (microCT) for laminar leaves from 23 species that represent a broad phylogenetic and anatomical spectrum. Importantly, the differential absorption of X-ray energy by water and air allows for segmentation and quantification of intercellular air space and thus S_m. Further, X-ray microCT effectively generates hundreds to thousands of 2D virtual leaf cross-sections with submicrometer thickness, providing the necessary data to compare both 3D estimates of IAS properties and established 2D methods using the same dataset. However, microCT as used here cannot distinguish chloroplasts and organelles, and thus cannot provide a direct estimate of S_c (e.g., see Ho *et al.*, 2016). Based on this analysis, we provide recommendations regarding the estimation of S_m using both 2D and 3D techniques, and guidelines for comparing values obtained in previous studies and setting a standard for future efforts.

Previous methods for estimating S_m

Here, we focused on four contrasting methods that estimate mesophyll surface area from cross-sections (see the Supporting Information Notes S1 for more detail):

- *Paradermal + cross-section (PCS).* Turrell (1936) provided the earliest method to estimate S_m, which was later applied in early landmark papers such as El-Sharkawy & Hesketh (1965). It uses paradermal slices from each cell layer and a cross-section to scale 2D sections to 3D, making basic assumptions about cell distribution in each layer, and requires a higher number of slices to estimate S_m.
- *Curvature correction factor (CCF).* Thain (1983) provided an easy method to apply a curvature correction based on cell geometry which was validated against stereological methods (Morris & Thain, 1983). This method can be used with cross-sections alone, although a combination of cross-sections and paradermal sections achieve the best results. It is currently the most commonly used method in the literature.
- *Oblique-paradermal section (OPS).* James *et al.* (1999) presented a method using only a single, oblique-paradermal section, which was subsequently used by Slaton & Smith (2002) to compare the leaf anatomy of 56 species from 21 families, but has not been adopted since, to our knowledge.
- *Regular geometrical shapes (RGS).* Sack *et al.* (2013) presented an updated method of Nobel *et al.* (1975) that quantifies mesophyll traits based on idealized cell shapes, while making the assumption that all mesophyll surface is exposed to the IAS.

As stereological methods have been less adopted and were used mainly to estimate cell properties in recent years (as opposed to whole mesophyll properties; e.g. Ivanova & P'yankov, 2002; Albrechtová *et al.*, 2007), we excluded this group from our analysis.

Materials and Methods

Comparing 2D and 3D estimates

Plant material Species were selected from various glasshouses and arboreta that represent a broad diversity of plant groups, leaf structure, and palisade tissue fraction (Table 1 and Supporting Information Table S1 for full names and growth location of the species). Only laminar leaves were selected for this study, which facilitated the computation of leaf area between the various methods. Such a comparison would have been less straightforward with needles or scale-like leaves with more complex geometries. A small group of *Bromeliaceae* was investigated to cover both C_3 and CAM leaf types and to compare both microCT and light microscopy methods. Healthy, well-watered plants were selected, and the petiole or stem was excised, wrapped in wet paper towels, and immediately put in plastic bags. They were transported and scanned at the microCT facility within 36 h.

Three-dimensional method: segmentation and classification of air space, mesophyll tissue, and veins from microCT scans Leaf samples were brought to the Advanced Light Source (ALS) at Lawrence Berkeley National Laboratory (LBNL; beamline 8.3.2) or to the Advanced Photon Source (APS) at Argonne National Laboratory (ANL; beamline 2-BM-A,B). The following steps were used to segment and classify the air space, mesophyll tissue, and veins, and are shown in Fig. 1:

Table 1 Anatomical data and mesophyll surface area exposed to intercellular air space per leaf area (S_m) values estimated using X-ray microcomputed tomography (microCT; three-dimensional, 3D) and two-dimensional (2D) methods for the 23 studied species

						$S_{m,3D}$		$S_{m,2D}$					Curvature correction		
Family	Species	t (μm)	θ_{pal}	θ_{sp}	f_{pal}	R1[a]	R2	RAW	OPS[b]	CCF	PCS	RGS	F_{pal}	F_{sp}	F_{leaf}
Pteridophytes															
Aspleniaceae	*Asplenium nidus*	128		0.25	0	11.1	9.6	8.6 (1.9)[c]	8.1	12.6	10.6	25.1		1.44	1.44
Polypodiaceae	*Platycerium bifurcatum*	380	0.05	0.24	0.43	19.6	16.5	13.6 (3.5)	16.9	18.2	17.2	57.8	1.39	1.33	1.33
Pteridaceae	*Adiantum tenerum*	220	0.50	0.62	0.13	25.9	22.2	15.1 (1.3)	16.9	22.4	20.8	14.2	1.36	1.50	1.48
	Myriopteris aurea	237	0.16	0.35	0.42	28.0	23.0	19.5 (1.6)	20.8	26.7	28.9	48.7	1.52	1.27	1.38
Gnetophytes															
Welwitschiaceae	*Welwitschia mirabilis*	670[d]	0.05		1	49.5	32.9	31.4 (2.8)	48.6	47.5	45.9	157.8	1.46		1.46
Magnoliids															
Lauraceae	*Cinnamomum verum*	95	0.15	0.60	0.22	9.5	8.0	6.8 (2.0)	6.7	8.7	8.8	24.6	1.49	1.20	1.26
Basal angiosperms															
Austrobaileyaceae	*Austrobaileya scandens*	228	0.05	0.17	0.29	8.2	7.3	6.0 (1.5)	7.9	6.8	8.3	53.3	1.36	1.23	1.26
Nymphaeaceae	*Nymphaea* × 'Pygmea helvola'	655	0.27	0.63	0.31	33.3	28.6	23.6 (2.4)	23.9	31.9	35.1	65.6	1.46	1.32	1.36
Schisandraceae	*Illicium floridanum*	257	0.25	0.51	0.31	13.4	12.2	9.6 (1.2)	9.8	12.2	12.0	21.0	1.42	1.21	1.28
Asterids															
Asteraceae	*Helianthus annuus*	210	0.24	0.45	0.55	24.5	19.9	17.1 (5.2)	20.1	24.0	24.8	53.1	1.51	1.31	1.42
Campanulaceae	*Brighamia insignis*	107	0.08	0.18	0.20	11.6	9.8	7.8 (1.4)	9.7	10.9	10.5	50.1	1.41	1.40	1.40
Ericaceae	*Rhododendron ciliipes*	340	0.08	0.38	0.50	27.3	19.8	18.1 (2.6)	22.7	25.5	30.3	65.6	1.52	1.33	1.43
Helwingiaceae	*Helwingia chinensis*	95	0.24	0.69	0.34	12.2	11.0	8.4 (2.0)	9.0	12.2	11.1	18.2	1.45	1.38	1.40
Rosids															
Malvaceae	*Gossypium hirsutum*	304	0.20	0.36	0.57	41.6	31.9	28.8 (5.9)	30.8	41.3	37.4	75.0	1.55	1.33	1.45
Rosaceae	*Prunus dulcis*	178	0.19	0.35	0.50	31.2	21.2	18.5 (3.9)	25.7	26.4	24.3	74.7	1.49	1.43	1.46
Monocots															
Araceae	*Monstera deliciosa*	165	0.14	0.40	0.26	18.6	16.8	11.5 (1.4)	14.9	14.7	17.0	40.4	1.46	1.22	1.28
Bromeliaceae	*Aechmea fendleri*	150		0.04	0	8.2	6.8	6.4 (0.8)	7.2	8.9	8.8	35.8		1.38	1.38
	Aechmea fulgens	459	0.10	0.71	0.90	39.2	29.2	30.0 (8.6)	27.2	37.8	–[e]	69.6	1.33	1.35	1.33
	Bilbergia elegans	380	0.06	0.74	0.74	29.1	22.7	19.1 (1.5)	16.4	24.9	–[e]	51.0	1.32	1.27	1.31
	Guzmania lingulata	99	0.07	0.64	0.26	9.6	8.0	6.4 (0.6)	6.3	8.1	10.3	23.5	1.41	1.22	1.27
	Nidularium innocentii	113	0.12	0.56	0.25	12.0	10.3	8.0 (1.4)	9.5	10.5	10.4	23.0	1.35	1.28	1.30
	Puya alpestris	322	0.09	0.30	0.25	37.5	28.6	25.1 (1.9)	33.9	33.3	30.8	91.8	1.44	1.30	1.33
Orchidaceae	*Oncidium ornithorhynchum*	151		0.04	0	16.4	9.7	10.8 (1.8)	6.9	13.1	10.6	60.2		1.22	1.22

[a]Resampling rate (R) used to produce the 3D surface: 1, smaller grid (more detail); 2, larger grid (smoother, but less detail).
[b]CCF, Thain's (1983) curvature correction; PCS, Turrell's (1936) paradermal + cross-section method; OPS, James *et al.*'s (1999) oblique-paradermal section method; RGS, Sack *et al.*'s (2013) regular geometrical shapes method.
[c]Standard deviation in parentheses. The same SD applies to the CCF values.
[d]Leaf thickness of *Welwitschia* is 1871 μm, but the mesophyll is only 670 μm.
[e]Because of the large lacunae and the organization of the cells within the leaf profile, it was not possible to apply the Turrell method properly for those species.

New Phytologist

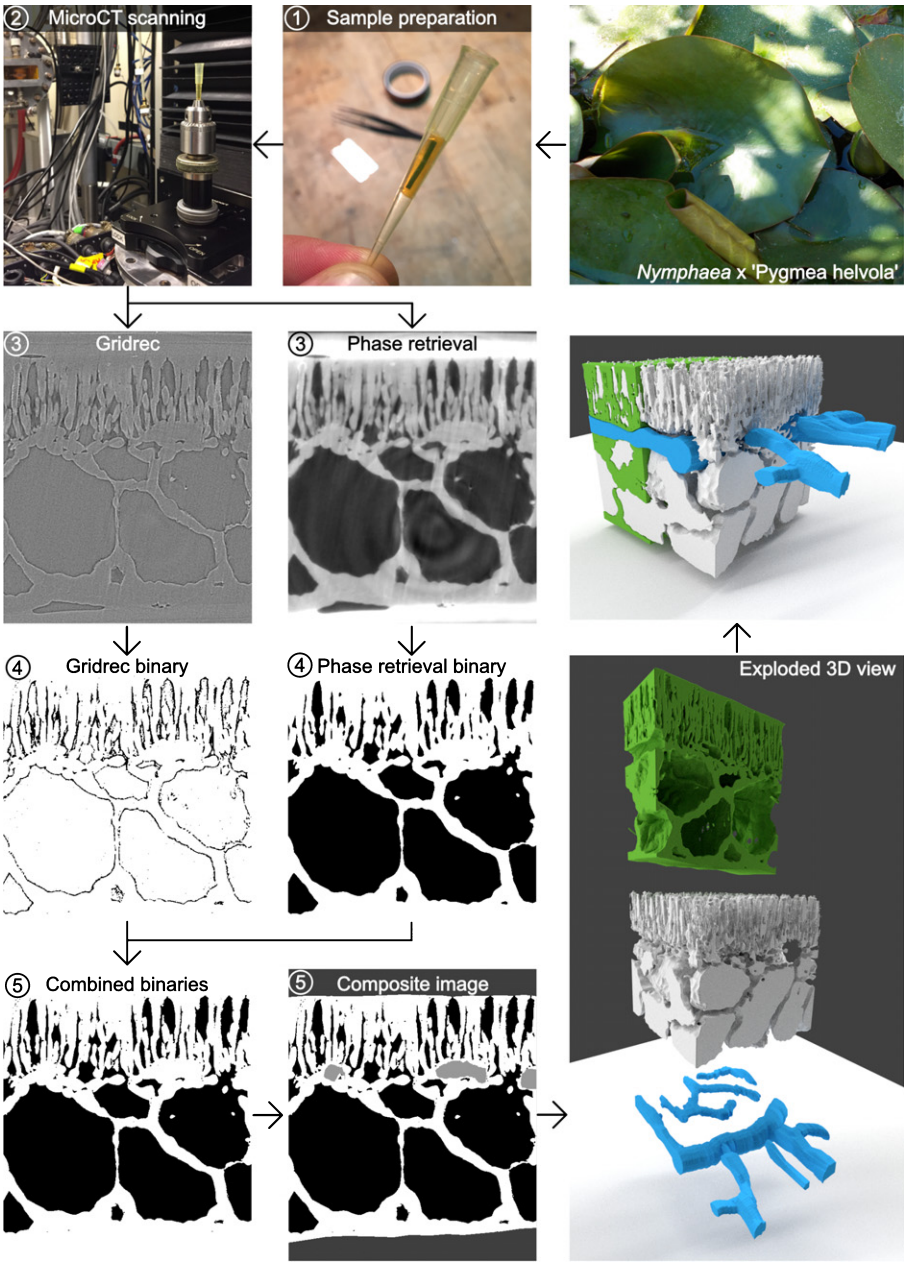

Fig. 1 Graphical representation of the steps needed to produce a three-dimensional (3D) representation of the leaf air space, from leaf sample preparation (1), X-ray microcomputed tomography (microCT) scanning (2; X-ray source entering through rectangular window on the left) to the creation of a composite image stack with leaf air space, cells, veins and mesophyll being segmented (3–5). The full description of the different steps is presented in the Materials and Methods section associated with the circled numbers. In the exploded three-dimensional (3D) view, veins are blue, intercellular air space is light gray, and cells are green.

1 *Sample preparation*. Before each scan (< 30 min), one *c*. 1.5- to 2-mm-wide and *c*. 20-mm-long sample was excised near a major vein from a fully developed leaf. Initial samples (run at ANL) were sealed in a pipette tip positioned above a water drop to prevent desiccation, but this sometimes resulted in flooded samples (samples not included here). Samples scanned at LBNL were enclosed between two pieces of Kapton (polyimide) tape to prevent desiccation while allowing high X-ray transmittance. The sample was then placed in the pipette tip and mounted and centered in the microCT X-ray beam.

2 *MicroCT scanning*. Samples were scanned using the CT mode capturing 1025 projection images at 21–25 keV, using either the ×5 or ×10 objectives, yielding a final pixel resolution of 1.28 and 0.64 μm, respectively (pixel resolution^3 = voxel volume of 2.10 and 0.26 μm^3, respectively). Scans were completed in *c*. 15 min.

3 *Reconstruction*. Reconstruction was carried out using *TomoPy*, a Python-based framework for reconstructing tomographic data (Gürsoy *et al.*, 2014). Each raw dataset was reconstructed using both the Gridrec (Dowd *et al.*, 1999) and phase retrieval reconstruction methods (Davis *et al.*, 1995), yielding complementary results. Gridrec performed better in isolating small pores and air–cell boundaries, but was less efficient in segmenting larger air voids, which were better isolated using phase retrieval reconstructions. Image stacks were rotated so that the leaf was oriented in a cross-sectional view and the epidermises were parallel to the image stacks' top and bottom borders, and such that their position was similar from the front until the end of the stack. When

possible, veins were aligned so that they were consistently positioned through the stack. We then cropped the tissue to focus on a region of interest between the middle of two major veins when present, so that the image was entirely mesophyll and excluded sample edges where desiccation occasionally occurred during sample preparation. The final stacks contained between 200 and 2000 8-bit grayscale images (down-sampled from 32-bit). Image processing was applied equally among scans using ImageJ software (Schneider *et al.*, 2012).

4 *Air space segmentation and classification.* The air space was segmented for each reconstruction method by visually and subjectively defining a range of pixel intensity values between a minimum and maximum grayscale value to optimize air space classification while minimizing false classification (i.e. nonair-space pixels). This resulted in a binary image stack that defined the presence or absence of air space.

5 *Combining classified images from both reconstruction methods and classifying other leaf features.* Binary image stacks from both reconstructions were combined using ImageJ's 'Image Calculator' function. To produce estimates of IAS features, the mesophyll boundaries were manually drawn as regions of interest (ROIs) for slices where significant changes occurred, and ROIs for in-between slices were interpolated using the 'Interpolate ROIs' function. The boundaries of all veins were segmented in the same manner, as were fibers if present. We removed the veins to avoid including that tissue as part of the total mesophyll volume and to avoid falsely classifying air-filled vessels as IAS. To produce the final stack before analysis, the area outside of the mesophyll and veins was classified with unique pixel values. We refer to this stack as the 'composite stack' (stack with cells, air space, veins, and other mesophyll), as opposed to 'binary stack' (air space and nonair space).

Three-dimensional method: measuring S_m and other IAS features from the image stack To extract the IAS features and measure S_m, the composite stack was prepared by selecting only the air space using the 'Threshold' function in ImageJ. With this binary stack, air space features were measured using 'BoneJ', an ImageJ plugin originally developed to analyze bone morphology (Doube *et al.*, 2010; all of the following functions were contained within this plugin). Air space volume and total volume of the sample were measured using the 'Volume fraction' function. Air space surface was measured using the 'Particle Analyzer' function. Potential signal noise was reduced by analyzing only 3D particles, i.e. a group of connected voxels, larger than three voxels ($3 \times$ pixel resolution^3 (μm^3)). To estimate IAS surface area, meshes, consisting of triangles of similar sizes connected through their edges, were produced around the IAS volumetric particles. The sizes of the triangles were adjusted by changing the resampling rate, the two lowest values of which were compared. A resampling rate of 1, the lowest possible value, results in a surface mesh with smaller triangles, and thus finer features are extracted. A resampling rate of 2 results in a smoother mesh with fewer triangles. The surface area of all the particles extracted by Particle Analyzer were summed and used as the total mesophyll area exposed to the IAS (A_{mes}, μm^2). Mesophyll volume (V_{mes}, μm^3) was computed from the total volume of the sample minus the vein volume. Leaf sample area (LA, μm^2) was defined as the image width multiplied by stack depth. $S_{m,3D}$ was then computed as:

$$S_{m,3D} = A_{mes}/LA \quad \text{Eqn 1}$$

Two-dimensional methods: estimating S_m using 2D methods for individual microCT slices For Thain's curvature correction (CCF method; Morris & Thain, 1983; Thain, 1983; Evans *et al.*, 1994), the average major (a; length) and minor (b; width/diameter) axes of at least 10 adjacent cells were measured within a randomly placed sampling window that included both palisade and spongy mesophyll in a representative cross-section slice from the Gridrec stack (Fig. 2). The curvature correction factor (F) was computed for each mesophyll tissue from the b/a ratio (Thain, 1983; see Methods S1 for the complete list of equations and accompanying R code, also available online at https://github.com/gtrancourt/curvature_correction), and the leaf-averaged F was computed as described in Evans *et al.* (1994):

$$F_{leaf} = F_{sp} \times f_{sp} + F_{pal} \times f_{pal} \quad \text{Eqn 2}$$

where f_{sp} and f_{pal} are the fraction of spongy and palisade mesophyll. This correction factor was applied to the uncorrected S_m data ($S_{m,RAW}$), which is the sum of the perimeter of each air space area in one single slice in cross-sectional view (P) divided by the width of the cross-section (w), such that the S_m values corrected for the curvature of the cells were:

$$S_{m,CCF} = (P/w) \times F_{leaf}. \quad \text{Eqn 3}$$

Note that individual $S_{m,RAW}$ (P/w) and $S_{m,CCF}$ values are available for hundreds to thousands of slices and, unless specifically stated, the median value for the entire stack is presented.

For the oblique-paradermal section method (OPS; James *et al.*, 1999; Slaton & Smith, 2002), a line selection was drawn on the binary stack from ad- to abaxial epidermis at an angle of *c.* 30° in a cross-sectional view, and an OPS was produced by reslicing the stack, i.e. generating a new 2D image composed of the pixel values along the line selection for each slice ('Reslice' function, without interpolation). The resulting image was binarized again ('Adjust threshold' function) because of gray-valued pixels produced with the 'Reslice' function. The perimeter of the air space in the OPS (P_{OPS}) was measured as described previously and S_m was estimated as described in Slaton & Smith (2002):

$$S_{m,OPS} = \frac{P_{OPS} \times t}{w_{OPS} \times L_{OPS}} \quad \text{Eqn 4}$$

where t is the thickness of the mesophyll, measured on the Gridrec reconstruction under a cross-sectional or longitudinal view, w_{OPS} and L_{OPS} are the width (along epidermis; from *c.* 400 to 1200 pixels) and length (from ad- to abaxial epidermis; from *c.* 800 to 2000 pixels) of the OPS (Fig. 2).

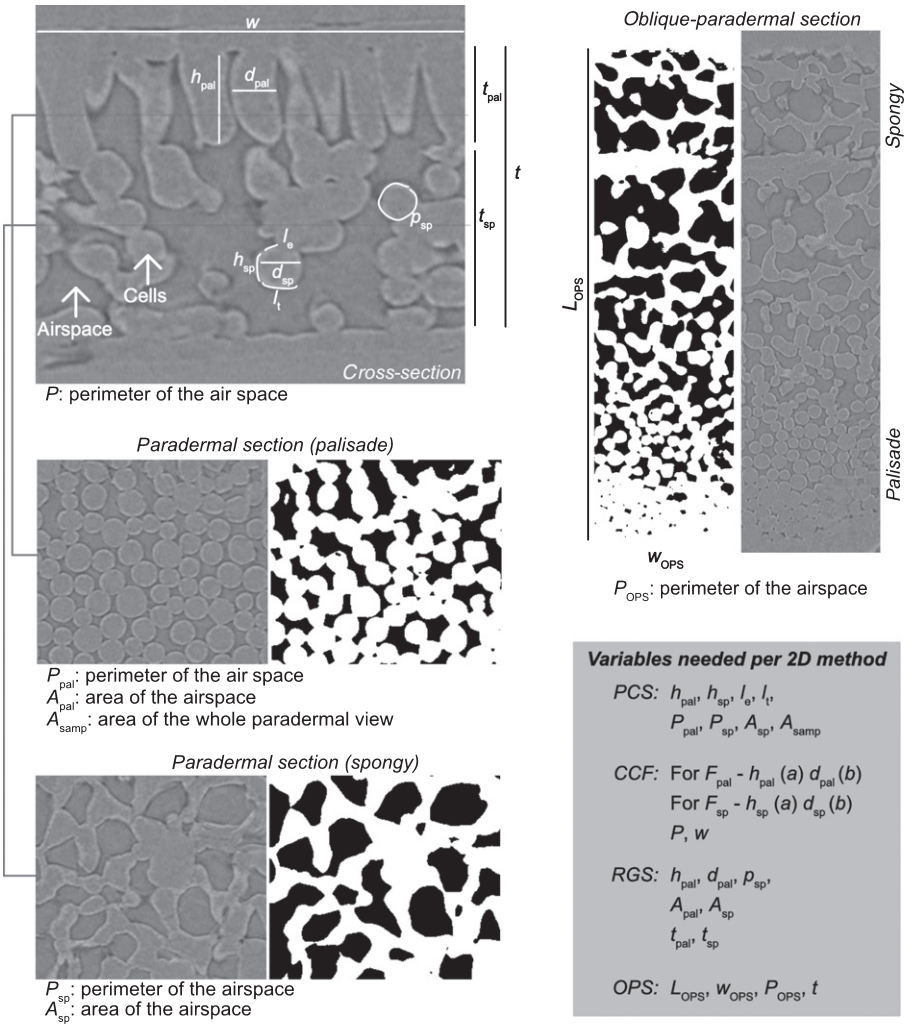

Fig. 2 Graphical representation of the different variables measured on two-dimensional (2D) sections for the four 2D methods compared in this study. For each section, the variables are drawn out when they are measured directly on cells or when corresponding to the dimensions of the section. Variables measured on binary images (air space and nonair space; examples presented for the paradermal and oblique-paradermal sections) are written below their respective sections. A full description of each variable is presented in the Materials and Methods section. Air space, dark or black regions; cells, light or white regions. Variables: h, height of a cell; d, diameter of a cell; l_e, exposed horizontal length of a cell; l_t, total horizontal length of a cell; p, perimeter of a cell; t, thickness of the mesophyll; P, perimeter of the air space; A, area of the air space; w_{OPS}, width of an oblique paradermal section; L_{OPS}, length of an oblique paradermal section. Subscripts: pal, palisade mesophyll; sp, spongy mesophyll; samp, whole section.

For the paradermal + cross-section method (PCS; Turrell, 1936), cell dimensions were measured on a cross-sectional view using the Gridrec stack and averaged over at least 10 adjacent cells in a sampling window. The cell perimeter exposed to IAS and cell areas were measured on a paradermal section of the binary stack (see Fig. 2 for all following variables). The palisade surface area was estimated by multiplying, for each layer, the height of layer ($h_{pal,i}$) by its perimeter exposed to the IAS ($P_{pal,i}$), measured under a paradermal view. For the spongy mesophyll, the vertical length of the cells (h_{sp}) was measured at an angle not greater than 45° from vertical (i.e. h_{sp} can be a curved line, to represent the whole exposed height of the cell). The horizontal (paradermal) length of the spongy cells was measured again at an angle not greater than 45° from horizontal and divided into the length exposed to the IAS (l_e) and the total length (l_t), so that the horizontal exposed area could be corrected for the actual fraction that is exposed to the IAS. The perimeter exposed to the IAS (P_{sp}) and area (A_{sp}) of the spongy mesophyll cells were measured on a representative paradermal slice, and the resulting area for one layer was multiplied by the average number of spongy cell layers (n_{sp}). Turrell (1936) also accounted for the surface of the abaxial epidermis exposed to the IAS, as he was interested in the evaporative surface (area of the sample under a paradermal view: $A_{samp} - A_{sp}$). He estimated S_m as:

$$S_{m,PCS} = \frac{\sum_{i=1}^{n_{pal}} h_{pal,i} P_{pal,i} + n_{sp}\left(h_{sp} P_{sp} + 2A_{sp}\frac{l_e}{l_t}\right) + \left(A_{samp} - A_{sp}\right)\frac{l_i}{w}}{A_{samp}} \quad \text{Eqn 5}$$

where n_{pal} is the number of palisade cells layers (all anatomical components are presented in Fig. 2). Note that the numerator is composed of the palisade (1st term in Eqn 5), spongy (2nd term in Eqn 5) and abaxial epidermis (3rd term in Eqn 5) components. As the comparison conducted here uses the entire exposed surface, the abaxial epidermis term is relevant, but this term could be removed if only chlorenchymous tissue is of interest. Note that Turrell (1936) applied a correction to the abaxial epidermis term by measuring the length of the inner wall of the epidermis in the cross-sectional view (l_i) as the width of the cross-section being measured (w). This might be less relevant, however, when using digital imaging where the section can be easily rotated so that $l_i \approx w$.

For the RGS method (Sack *et al.*, 2013), cellular dimensions are used to compute each cell's surface area and volume, which are used to estimate the number of cells per tissue. Spongy mesophyll cells are assumed to be spheres with a circumference equal to the cell perimeter (p_{sp}), measured on a cross-section of the Gridrec stack. Palisade cells are assumed to be cylinders with hemispherical ends, and the length (h_{pal}) and diameter (d_{pal}) axes were measured on a cross-sectional view (Fig. 2). The surface of mesophyll per leaf area is then computed as:

$$SA_{pal} = 2\pi\frac{d_{pal}}{2h_{pal}},\ V_{pal} = \pi\left(\frac{d_{pal}}{2}\right)^2\left(\frac{4}{3}\times\frac{d_{pal}}{2} + h_{pal} - d_{pal}\right)$$

$$SA_{sp} = 4\pi\left(\frac{p_{sp}}{2\pi}\right)^2,\ V_{sp} = \frac{4}{3}\pi\times\left(\frac{p_{sp}}{2\pi}\right)^3$$

$$S_{m,RGS} = \frac{\overline{SA}_{pal}\times t_{pal}(1-\theta_{pal})}{\overline{V}_{pal}} + \frac{\overline{SA}_{sp}\times t_{sp}(1-\theta_{sp})}{\overline{V}_{sp}} \quad \text{Eqn 6}$$

where SA and V are the surface area and volume of one cell, and θ is the porosity of the tissue (area IAS (μm^2) / mesophyll area (μm^2)).

Identifying the minimum number of slices required to produce a reliable S_m estimate

Using the data from each individual slice (i.e. all $S_{m,RAW}$ values for one leaf), we estimated the number of 2D sections needed to estimate S_m within 5% or 10% of the leaf-level median with 95% confidence. To do so, we reordered the S_m values for each species to create 10 000 random sets. The median value was then calculated for each reordered set for an increasing number of slices, using only one S_m value up to 500 times or the maximum number of slices for that species, whichever was reached first. The 5th and 95th confidence intervals were computed, and the smallest number of slices needed to be within 5% and 10% was computed using R v.3.3.3 (R Core Team, 2017).

Comparing light microscopy to 3D data

Bromeliaceae leaf samples, from the same leaf scanned with microCT when possible, were prepared for microscopy following Bozzola & Russell (1999) and Russin & Trivett (2001). Leaves were fixed in Karnovsky's fixative, and then rinsed with 0.1 M phosphate buffer (pH 7.2) and postfixed for 2 h in 1% buffered osmium tetroxide. Leaves were dehydrated with ascending concentrations of ethyl alcohol with three changes at 100%, transitioned 1 : 1 with propylene oxide, and dehydrated using two changes of pure propylene oxide. Infiltration began using Epon/Araldite resin (EMS, Hatfield, PA, USA) in three ascending concentrations with propylene oxide. Finally, three changes of resin with microwave assistance were done before overnight polymerization in capsules. Semithin sections were cut using a Leica Ultracut UCT ultramicrotome and were stained with 2% Methylene Blue/Azure II before being observed at ×200 magnification with an Axio Imager A2 microscope (Zeiss, Oberkochen, Germany).

Structural traits, t, θ_{IAS}, P, w, and the total area of the mesophyll (A_{mes}; not including vein area), were analyzed using ImageJ software. To normalize for uneven leaf thickness between the embedded section and the microCT stack, the ratios $P/A_{mes,2D}$ ($\mu m\ \mu m^{-2}$; see also Nelson *et al.*, 2005) and $A_{mes,3D}/V_{mes,3D}$ ($\mu m^2\ \mu m^{-3}$) were compared.

Results

The 23 species analyzed spanned a broad range of mesophyll thickness (95–670 μm), porosity and fraction of palisade tissue within the leaf, from the spongy-only fern *Asplenium nidus* and the CAM orchid *Oncidium ornithorhynchum*, to the palisade-only *Welwitschia mirabilis* (Table 1). Using the microCT data, S_m ($S_{m,3D}$) was estimated with two resampling rates. A resampling rate of 1 (R1) produced $S_{m,3D}$ ($S_{m,3D\text{-}R1}$) values 10–70% higher (average 25%) than when using a resampling rate of 2 (R2; $S_{m,3D\text{-}R2}$). R2 produced a smoother surface mesh by using larger triangles, but this resulted in the exclusion of small air space volumes – an example of the coastline paradox (Mandelbrot, 1967). Consequently, small-diameter pores, i.e. close to the resolution limit of our images, were captured less accurately at a higher resampling rate. *O. ornithorhynchum* showed the largest difference between R1 and R2, where the mesophyll consists of tightly packed spheroids with a very low porosity (0.04) and narrow air passages. Leaves with packed palisade cells of small diameter, such as *Gossypium* and *Prunus*, also showed a large difference between R1 and R2. Further, a smaller resolution (or higher magnification) generally led to a larger difference between R1 and R2 (+27% with a magnification of ×5, or 1.28 μm pixel^{-1}, vs +19% with a magnification of ×10, or 0.64 μm pixel^{-1}).

The $S_{m,RAW}$ values, i.e. the uncorrected length of mesophyll exposed to the IAS divided by the section width, had a median value of 16% less than $S_{m,3D\text{-}R2}$ and 32% less than $S_{m,3D\text{-}R1}$ (Fig. 3). The OPS method produced $S_{m,2D}$ estimates with slightly less difference than with $S_{m,3D}$ values (−26% vs R1 and −8% vs R2; Fig. 3), yet the estimates were in a broader range than $S_{m,RAW}$. The RGS method, which estimates the entire cell surface and assumes that it is completely exposed to the IAS, produced $S_{m,RGS}$ values having a median +157% from the $S_{m,3D\text{-}R1}$, with values ranging from −52% to +552% (Table 1; Fig. 3). Of all the methods and resampling rates, only $S_{m,OPS}$ compared with $S_{m,3D}$ at R2 had similar means (one-sample t-test, $P = 0.23$), while the rest were significantly different (one-sample t-test, $P < 0.01$).

$S_{m,CCF}$ and $S_{m,PCS}$ values were similar to each other and most closely matched the 3D values, being within a median ±10% of the 3D values, for both R1 and R2. Generally, the species that were corrected to be within 10% of the $S_{m,3D\text{-}R1}$ value with Thain's CCF method had a similar difference when comparing the estimates from Turrell's PCS method. However, several species had better estimates with the PCS method than with the CCF method (e.g. *Monstera*, *Guzmania*, *Austrobaileya*; see Table 1). All leaf types performed well with both CCF and PCS methods, where, for example, leaves with high porosity (e.g. *Helwingia* and *Nymphaea*) and low porosity (e.g. *Aechmea*

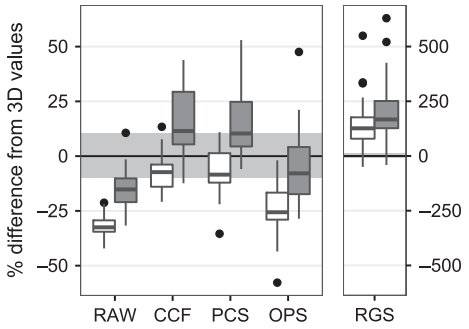

Fig. 3 Error associated with different methods for estimating the mesophyll cell surface area exposed to the intercellular air space per leaf area (S_m). Values estimated using two-dimensional (2D) methods are compared with the X-ray microcomputed tomography (microCT)-derived three-dimensional (3D) values obtained using a finer mesh size (resampling rate of 1; white boxes) and a slightly larger mesh size (resampling rate of 2; gray boxes). The raw and uncorrected 2D S_m values (RAW) are presented as a comparison: the curvature correction was applied to these values. The horizontal solid line represents no difference between the 2D and 3D estimates, and the horizontal light gray shaded area represents 10% below and above the 3D value. Of all the methods and resampling rates, only $S_{m,OPS}$ compared with $S_{m,3D}$ at R2 had similar means (one-sample *t*-test, $P = 0.23$), while the rest were significantly different (one-sample *t*-test, $P < 0.01$). Boxplots represent the median, first, and third quartiles, the ends of the vertical lines represent the 1.5 × interquartile range, and black points are outliers. $n = 23$, except for the PCS method where $n = 21$ as this method was difficult to apply to leaves with large lacunae. Note the difference in scale between the RGS, estimating the total mesophyll surface, and the other methods. CCF, Thain's (1983) curvature correction; PCS, Turrell's (1936) paradermal + cross-section method; OPS, James *et al.*'s (1999) oblique-paradermal section method; RGS, Sack *et al.*'s (2013) regular geometrical shapes method.

fendleri and *Platycerium*, both CAM plants) were within 10% of the $S_{m,3D\text{-}R1}$ value.

For most species (15 out of 23), one to three sections were necessary to estimate $S_{m,2D}$ within 10% of the whole sample median, 95% of the time (Fig. 4). For those species, a few more slices were needed to be within 5% of the leaf median and up to a total of 10 slices. The species that needed the highest number of slices to be within 10% of the leaf median (> 4 and up to 10) required substantially more slices to be within 5% (13 and up to 35). Those species were mainly eudicots with reticulate vein networks with no preferred orientation, or species with greater heterogeneity among slices (see Fig. 5). However, when the slices with a high proportion of veins were removed, a common subjective practice when analyzing microscopic slices, the minimum number of slices typically decreased substantially, with, for example, a decrease from eight to two slices for *Gossypium* (Fig. 4), leading to a narrower range of $S_{m,2D}$ values (Fig. 5). In comparison, *Myriopteris*, which needed only one slice to be within 10% of the leaf median, was very homogenous throughout the leaf sample (Fig. 5).

Finally, we compared light microscopy images for six bromeliad species to the microCT-derived 3D values. As the mesophyll thickness was different between the embedded and microCT samples, we applied a Thain (1983) curvature correction factor to the total perimeter of mesophyll measured per mesophyll area and not per leaf area. These data showed good agreement in relation to the mesophyll surface area over mesophyll volume ratio (Fig. 6a). Interestingly, the species that had the largest difference between the 2D and 3D values were the thickest leaves (*c.* 400 μm), while the thinnest leaves (*c.* 100 μm) produced very similar 2D and 3D values (Fig. 6b). Species with thicker leaves resulted in up to *c.* 40% less surface being estimated from embedded material compared with the 3D data using R1.

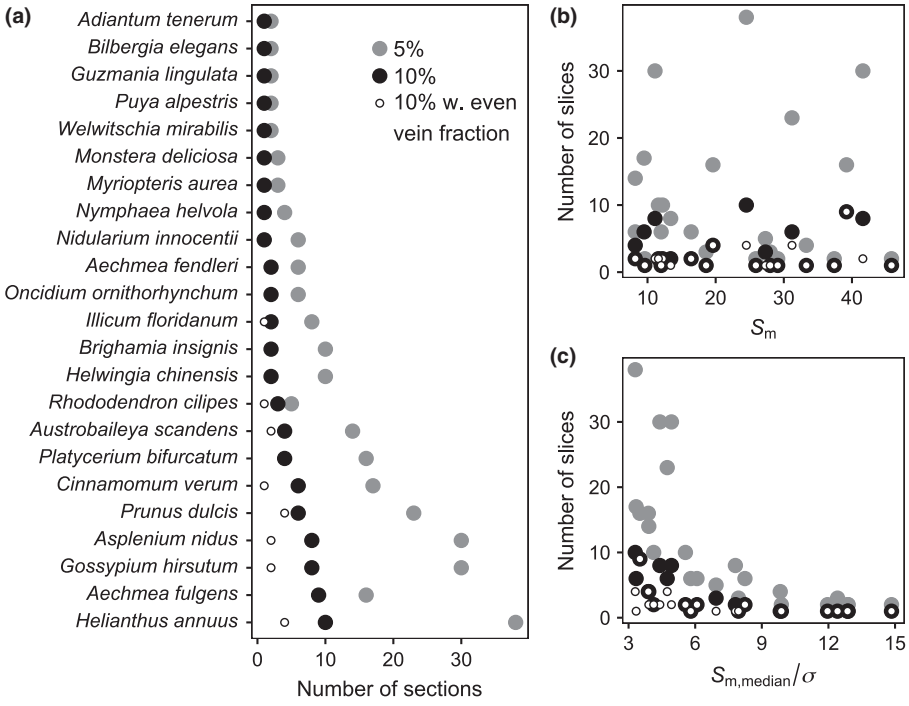

Fig. 4 (a) Number of two-dimensional (2D) sections needed to estimate the mesophyll cell surface area exposed to the intercellular air space per leaf area (S_m) within 5% (gray circles) or 10% (black circles) of the leaf-level median with 95% confidence; (b) relationship between the minimum number of slices and the median S_m values; (c) relationship between the minimum number of slices and the median S_m/standard deviation, σ. The minimum number of slices was also evaluated by removing the slices with too much vein coverage, a practice usually done on microscopic slices (small white circles in left plot, only when there was a different value from the black circles). This practice led to a substantial reduction in the minimum number of slices needed to get within 10% of the leaf-level median for most of the studied species.

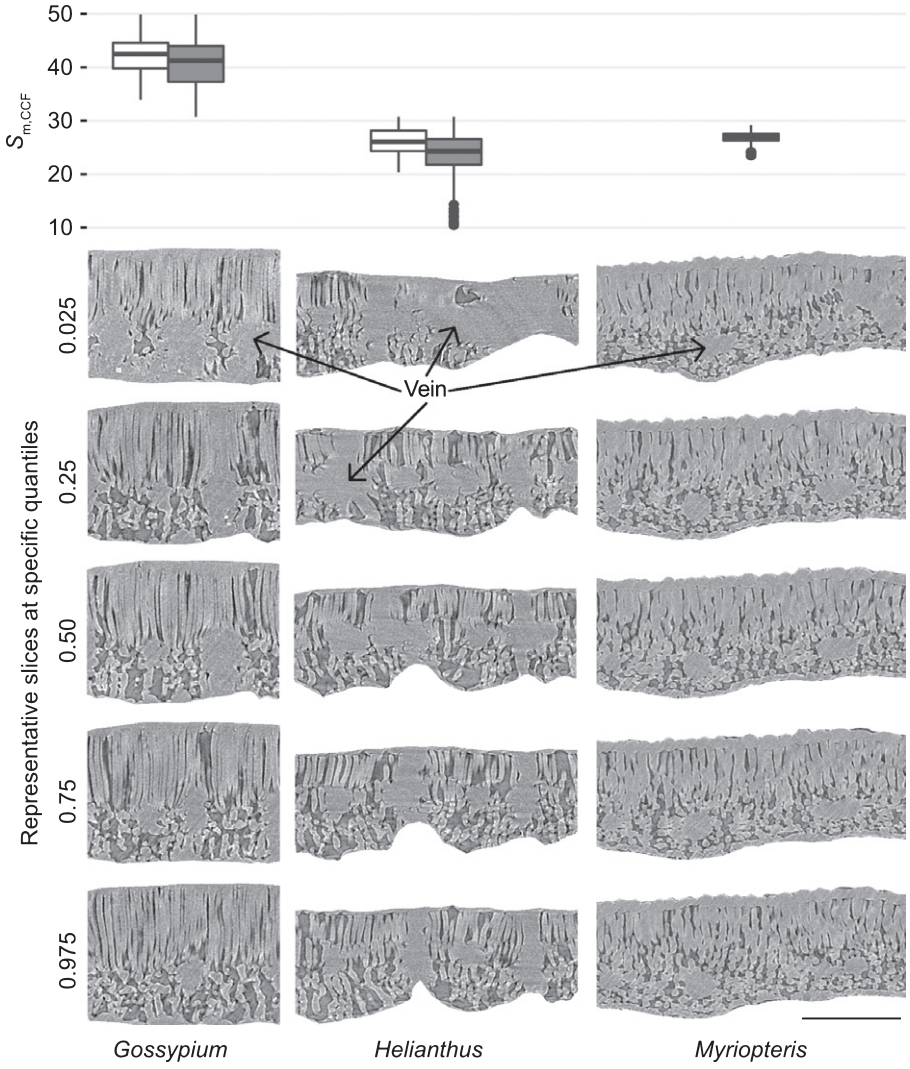

Fig. 5 The effect of vein area in the calculation of the mesophyll cell surface area exposed to the intercellular air space per leaf area (S_m) using the curvature correction factor (CCF) method. Boxplots show the distribution of S_m values calculated from images with (gray) and without (white) slices with a high fraction of vein tissue for *Gossypium*, *Helianthus*, and *Myriopteris* (boxplots represent the median, first, and third quartiles, the ends of the vertical lines represent the 1.5 × interquartile range, and black points are outliers). Representative transverse X-ray microcomputed tomography (microCT) slices at five quantiles (0.025, 0.25, 0.5, 0.75, 0.975) within the image stacks are shown, with veins being shown for each species. As the veins and cells are water-filled, thus having the same density under X-rays, they are not easily distinguishable from each other and one must look for the subtle cell walls to identify them. We have indicated with arrows the location of some of them. Scale bar: 250 μm.

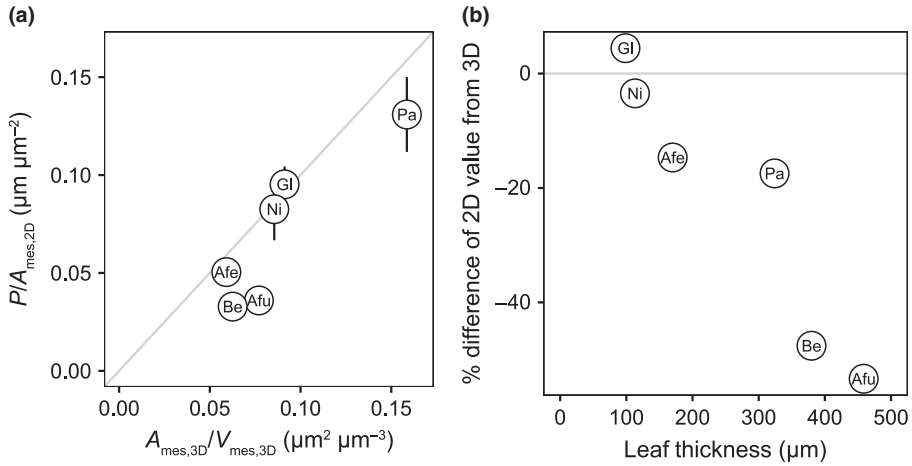

Fig. 6 Deviation of two-dimensional (2D) estimates of mesophyll surface area exposed to the intercellular air space (IAS) compared with the X-ray microcomputed tomography (microCT)-derived three-dimensional (3D) value, and how the error increases with leaf thickness. (a) The relationship between the 2D-derived mesophyll perimeter exposed to the IAS (P) relative to leaf area per total mesophyll area in the measured area ($A_{mes,2D}$) and the 3D equivalent derived using microCT: the surface of mesophyll exposed to the intercellular air space per total mesophyll volume ($A_{mes,3D}/V_{mes,3D}$). The same leaves were used for both X-ray microcomputed tomography (microCT) and light microscopy analyses, and 2 × standard deviation is presented for the 2D data obtained from multiple sections. (b) Relationship between leaf thickness and the relative difference between the 2D and 3D values. Afe, *Aechmea fendleri*; Afu, *Aechmea fulgens*; Be, *Bilbergia elegans*; Gl, *Guzmania lingulata*; Ni, *Nidularium innocentii*; Pa, *Puya alpestris*.

Discussion

Three-dimensional values as a reference, and a standardized method for the analysis of leaf microCT scans

Our use of microCT allows for a more geometrically accurate investigation of both plant structure and function, and an in-depth investigation into how close 2D estimates match the 3D geometry of complex surfaces within the leaf. Here, we present a method for extracting leaf air-space features and for estimating S_m, an important leaf trait that determines internal gas exchange and photosynthetic capacity.

Using microCT on fresh leaf samples allowed us to more fully capture the 3D mesophyll surface exposed to IAS without the potential artifacts associated with traditional light microscopy sample preparation, while at the same time removing the need to correct for cell curvature and complex geometry. In this way, we could measure volumetric features such as porosity of the air space, mesophyll volume, and vein volume. Other features could be measured, such as individual cell volume and surface area, by hand-drawing the contour of cells. One other advantage of the microCT leaf scans is that they can be used to generate volumetric meshes, i.e. a simplified rendering of a 3D object by approximating the volume as a collection of interconnected tetrahedra, for use in finite element modeling, as shown in Ho *et al.* (2016). Using microCT also has the advantage of being able to measure larger samples (slightly over 1 mm^3) nondestructively as compared with nonCT 3D techniques such as confocal microscopy, which has good accuracy for samples of *c.* 40 μm thick (Lhotáková *et al.*, 2008). However, nonCT 3D methods use instruments that are more readily available, such as confocal microscopy, and can produce comparable data as those from microCT. At the same time, such methods require a smaller sample size (Wuyts *et al.*, 2010) and are subject to artifacts that may result from fixation, clearing, staining, and other histological treatments.

Limitations do exist when using microCT for quantifying leaf anatomical traits. One limitation is the speed of scanning. Synchrotron microCT instruments are probably the most efficient because of the very high-energy flux of the X-rays, making a scan possible in < 20 min, compared with up to 12 h on a commercial machine for a comparable scan (Yannick Staedler, University of Vienna, pers. comm.). Such time savings can significantly reduce potential imaging artifacts as a result of tissue movement or dehydration. Magnification is also a potential limitation which typically does not exceed a resolution of *c.* 0.3 μm $pixel^{-1}$ (the resolution available for the present study was 0.64 and 1.28 μm $pixel^{-1}$, resulting from different magnification settings used during microCT scanning). Using light microscopy, this can be substantially lower depending on the microscope, which can show minute details that cannot be seen using microCT. Wuyts *et al.* (2010) presented a nonCT 3D method using confocal microscopy that allows imaging of leaves at a higher magnification and with high-cell contrast, and as such provided higher-quality images than microCT. However, their method uses cleared, stained leaves, i.e. leaves were bleached to increase light penetration. This comes with an associated tradeoff of losing Chl that is needed to identify chloroplasts. Furthermore, the leaf samples are stored and analyzed in ethanol, which can cause distortion in the cells as compared with fresh samples that are used in microCT (Uwins *et al.*, 1993; Talbot & White, 2013).

Another important limitation of microCT is its inability to detect organelles. Contrast in X-ray images is largely determined by differences in X-ray attenuation within the sample. As the contents of water-filled plant cells generally do not show differential absorption of X-rays, the interior of cells typically appears to be homogenous with microCT images, although the higher density of cell walls makes it possible to delineate individual mesophyll cells (Fig. 1). Light microscopy has the advantage of allowing researchers to distinguish among chloroplasts, organelles and compounds through the staining of sections. Hence, without prior knowledge of a leaf's anatomy, it is impossible to accurately identify the chloroplasts' distribution in a microCT scan, which probably needs to be combined with a stained cross-section to identify these tissues (e.g. Ho *et al.* (2016) created artificial organelles based on light microscopy to populate their cells for modeling). Finding suitable X-ray contrast agents could facilitate the extraction of specific membranes and organelles, along with improving the contrast between the air space and the cells, as was done with flowers (Staedler *et al.*, 2013). NonCT 3D techniques, such as fluorescence confocal microscopy, allows the user to distinguish cell walls and chloroplasts easily (Kubínová *et al.*, 2014), which could be used to produce volume-based S_c estimates, although this has not been done to our knowledge. However, the chloroplast surface from confocal microscopy obtained through autofluorescence of Chl, for example, is not as well defined compared with electron microscopy images. Techniques new to plant biology, such as focused ion beam scanning electron microscopy (Oi *et al.*, 2017) or serial block face scanning electron microscopy (Kittelmann *et al.*, 2016), would allow for 3D estimates of S_c and to produce high-resolution surface meshes at the cellular level for finite element modeling. Ultimately, some combination of these complementary methods will be needed to measure and model these traits as they span several orders of magnitude in size yet are interdependent, and no single method is currently capable of extracting all the necessary detail.

A general limitation of 3D methods, both microCT and nonCT methods, is related to the volume rendering in the computer analysis of the image stacks, and especially the size of the mesh to represent the mesophyll–air space surface interface. This size is controlled by changing the resampling rate in BoneJ, and decreasing the resampling rate renders a finer mesh with more triangular facets. Using the smallest value, 1, results in a more jagged rendering, but more accurately represents the original geometry, while increasing the resampling rate increases triangle size and hence smooths the rendered surface. Thus, it is essential to report this rate and to investigate if there are substantial differences between the two rates (e.g. Fig. 3). However, all of our intermethod analyses were done with consistent resampling rates, avoiding scale-dependent differences.

Although using a smaller resampling rate leads to a more accurate representation of the air space, a smaller mesh size requires

greater memory for processing the stack. For example, using the Particle Analyser function of BoneJ to analyze the surface area of the *Gossypium* image stack (file size of 56 Mb) required *c.* 1.7 Gb of RAM for R1 (30 times the file size for 17.16×10^6 triangles) and *c.* 800 Mb of RAM for R2 (14 times the file size for 3.31×10^6 triangles; analysis ran on a 2.6 GHz Intel Core i7 laptop with 16 Gb of RAM). The average file size was between 500 and 700 Mb, and those were easy to process on the laptop described. However, some stacks were over 1 Gb in size, and to analyze those in their entirety we had to rely on a virtual machine (eight cores and 64 Gb of RAM), and it still led to over 50 Gb of RAM being used.

Critical evaluation of methods applied to leaf sections and the validity of 2D analyses

Several methods have been presented in the literature since Turrell's (1936) method to estimate S_m. Yet no critical evaluation has been carried out (Sack *et al.*, 2013). The increasing availability of large leaf trait databases (e.g. TRY database; www.try-db.org) and efforts to discover more general relationships among leaf traits (e.g. Onoda *et al.*, 2017) highlight the need for methodological standardization. The four methods evaluated here produced substantially different results relative to 3D values (see Table 1; Fig. 3). Unsurprisingly, the method which measures the entire cellular surface (RGS; Sack *et al.*, 2013) produces the highest discrepancies. Of the three other methods, Thain's (1983) CCF and Turrell's (1936) PCS stand out for how well they approximate 3D values, often within 10% of the 3D S_m at a R1, which we consider the standard in this study. The PCS method produced the most accurate estimates, typically within 10% of $S_{m,3D\text{-}R1}$ (15 out of 23; 65%). However, Turrell's method necessitates a large number of sections. While it was easy to virtually slice through each palisade layer with our 3D image stack, doing so with an embedded sample requires more expertise, especially when cutting precisely though each layer. We thus recommend this method for users who are very experienced with anatomical techniques or when a small sample size allows for more meticulous work.

The CCF (Thain, 1983) method is not a measurement technique like the PCS method (Turrell, 1936), but instead applies a generic correction factor (F) to adjust the length of mesophyll perimeter exposed to the IAS to account for the curvature of cell walls within the section. A curvature correction could be applied to each cell, but usually only one correction factor is used for the whole leaf section. This correction factor is typically the average of the palisade and spongy F-values (Evans *et al.*, 1994; Galmés *et al.*, 2013; Théroux-Rancourt & Gilbert, 2017). The CCF method is the most commonly used method to produce S_m estimates in recent years. While fewer $S_{m,CCF}$ estimates fell within 10% of $S_{m,3D\text{-}R1}$ compared with PCS (13 out of 23; 57%), it requires low effort to produce relatively reliable estimates.

We further compared our 3D estimates with embedded leaf samples typical of light microscopy. As microCT samples and the sections from embedded material often presented different leaf thicknesses, we compared the length of mesophyll exposed to the IAS over the mesophyll cross-sectional area ratio, as suggested for CAM plants (Nelson *et al.*, 2005). This allowed us to standardize the actual exposed surface per unit mesophyll cross-sectional area. Using the same leaf, 2D estimates acquired from embedded material showed good agreement with 3D values in thin leaves (*c.* 100 μm), while they diverged as the leaves became thicker (*c.* 400 μm) (Fig. 6). The more important deviations between the embedded and microCT results could be explained in several ways. First, thick leaves tended to be CAM-type, which can be more difficult to embed and section as a result of their weaker cell walls, thicker cuticles, and a high fiber content. This could distort leaf thickness by compressing cells, thereby leading to less surface being measured. There are limited reports regarding the presence of distortions and shrinkage of cells following the embedding of plant leaves (Uwins *et al.*, 1993; Winter *et al.*, 1993; Talbot & White, 2013), and this effect might be amplified in CAM leaf samples. Further, thicker leaves might be more prone to anatomical variations between the leaf sections, which, over such a volume, might lead to greater variation in the amount of exposed surface. However, the differences are not caused by the user analyzing the embedded slice, as both lead authors independently measured values within 5% of each other using two different approaches (data not shown).

Ultimately, our data suggest that, for most species, traditional light microscopy with Thain's CCF method would lead to reliable S_m values within an acceptable range of microCT values. Thus, the published relationships between S_m (and consequently S_c) estimated using the CCF method and A_{max} or g_m would remain valid (e.g. Evans *et al.*, 1994; Tholen *et al.*, 2008; Tosens *et al.*, 2016). This does not necessarily mean that relationships obtained with the RGS methods are not valid. This method, estimating the total mesophyll surface as opposed to the surface exposed to the IAS, was used to present strong relationships with A_{max} (e.g. Nobel *et al.*, 1975; Chatelet *et al.*, 2013). While the total mesophyll area per leaf area is a relevant trait to measure, it leads to substantially higher values than with the other methods that explicitly measure the mesophyll surface exposed to the IAS. Consequently, measurements made using the RGS method should not be compared with the others. Fortunately, a recent report made this distinction (Onoda *et al.*, 2017). To avoid confusion, we recommend using A_{mes}/A when the total mesophyll surface is measured, and defining S_m as the surface area exposed to the IAS, as this has been used in the most cited references (e.g. Evans *et al.*, 1994).

More replications needed for leaves with reticulate vein network

Using our binary stacks of microCT leaf cross-sections, we showed that for *c.* 40% of the studied species, only one section was needed to produce an $S_{m,CCF}$ estimate within 10% of the whole leaf median, 95% of the time (Fig. 4a), and 65% of the species need three slices or fewer. A common practice is to measure S_m over at least three slices (e.g. Evans *et al.*, 1994; Tholen *et al.*, 2008; Tosens *et al.*, 2012). Hence, for a high number of species, averaging S_m from at least three slices would provide

estimates close to the leaf median. However, several species had to be averaged over a higher number of slices to get an S_m value within 10% of the leaf median. This was not related to the raw S_m value (Fig. 4b), but rather to the anisotropy in leaves found in certain species with reticulate leaf veins (e.g. Fujita & Mochizuki, 2006). Looking more closely at the species differences, we found that those needing the fewest slices were mainly parallel-veined leaves such as monocots, or species with a low-density reticulate vein network (e.g. *Myriopteris* and *Nymphaea*). For species possessing a dense, reticulate vein network, the number of slices had to be increased substantially, requiring up to 30 slices if the goal was to reach within 5% of the leaf median. Fortunately, those outliers were caused by a high proportion of vein in the slices (Fig. 5), which were included in our method automated over the whole leaf stack, and this becomes obvious when one examines the relationship between the number of slices and the ratio of the $S_{m,2D}$ median and standard deviation (Fig. 4c). Ultimately, it is up to the person doing the study to determine how many slices he or she needs. Our case is an exception as we compared a minimum of 200 slices. In doing this, we identified that removing the slices with a substantial vein fraction, a common yet subjective practice, decreased the number of slices needed, resulting in 83% of species requiring three slices or fewer to be within 10% of the leaf median. However, one might look at 10 slices, for example, and find that variability is high, which would suggest that more slices are needed.

Conclusion and recommendations for the use and reporting of 2D methods

We describe in this paper a method to reconstruct, extract, and analyze plant leaves scanned with microCT, based entirely on open-source software. For a diverse anatomical and phylogenetic set of 23 species, we compared our 3D S_m estimates with four 2D methods commonly found in the literature – treating the microCT stacks as a digital leaf sample, a most appropriate tool for this comparison. The RGS method (e.g. Sack *et al.*, 2013) produces the highest discrepancy as it estimates the entire cell surface and not just the surface exposed to the IAS. The PCS method (e.g. Turrell, 1936) is the most accurate as it often estimates 2D S_m to within 10% of the 3D value, but it necessitates the highest number of leaf sections, both cross-section and paradermal. The CCF method (e.g. Thain, 1983) is the easiest to apply and produces reliable estimates, and so would be the method of choice for most researchers without access to microCT. The CCF method also produces reasonable results when comparing with embedded leaf samples, the most common way of estimating S_m in the literature, and it can easily be applied to needles or scale-like leaves as it only corrects the measured surface within the section, as opposed to the PCS method which was intended for laminar leaves. Hence, the CCF and PCS methods are valid and comparable between themselves, and they should be the only methods used when comparing data from different sources in the literature. Moreover, to improve the reporting and quality of S_m estimates, we recommend that at least three cross-sections are averaged when using 2D methods, and more sections might be needed when analyzing species with reticulate veins, depending on the homogeneity in the fraction of vein coverage on the different slices. Regarding notation, we recommend reporting A_{mes}/A when the total mesophyll surface is measured (e.g. Nobel *et al.*, 1975; Sack *et al.*, 2013), and defining S_m as the surface area exposed to the IAS. Finally, when applying the CCF method, we suggest that authors measure and report curvature correction factors for each tissue, as opposed to using existing values in the literature.

Acknowledgements

We thank Pat Kysar for preparing embedded leaf cross-sections, Adam Roddy, Ernesto Sandoval (UC Davis Botanical Conservatory), Sandra Suwanski (University of Chicago), and Holly Forbes (UC Berkeley Botanical Garden) for material collected, and Danny Tholen for helpful discussions on Thain's equations. Xianghui Xiao assisted all scanning performed at the Advanced Photon Source (ANL). G.T-R. was supported by a Katherine Esau Postdoctoral Fellowship and a postdoctoral scholarship from the Fonds de recherche du Québec – Nature et technologie. J.M.E. was supported by NSF grant no. 1656610. The Advanced Light Source (ALS) is supported by the Director, Office of Science, Office of Basic Energy Sciences, of the US Department of Energy under contract no. DE-AC02-05CH11231.

Author contributions

G.T-R. and J.M.E. conceived the study, developed the method and analyzed the data, with methodological inputs from M.A.Z., C.R.B. and M.E.G. G.T-R, J.M.E., C.K.B., M.A.Z., A.J.M. and C.R.B. acquired the data. G.T-R. and J.M.E. wrote the manuscript, with contributions from all authors.

References

Albrechtová J, Janáček J, Lhotakova Z, Radochova B, Kubínová L. 2007. Novel efficient methods for measuring mesophyll anatomical characteristics from fresh thick sections using stereology and confocal microscopy: application on acid rain-treated Norway spruce needles. *Journal of Experimental Botany* **58**: 1451–1461.

Bozzola JJ, Russell LD. 1999. *Electron microscopy: principles and techniques for biologists.* Sudbury, MA, USA: Jones & Bartlett Learning.

Chabot BF, Chabot JF. 1977. Effects of light and temperature on leaf anatomy and photosynthesis in *Fragaria vesca*. *Oecologia* **26**: 363–377.

Chatelet DS, Clement WL, Sack L, Donoghue MJ, Edwards EJ. 2013. The evolution of photosynthetic anatomy in *Viburnum* (Adoxaceae). *International Journal of Plant Sciences* **174**: 1277–1291.

Davis TJ, Gao D, Gureyev TE, Stevenson AW, Wilkins SW. 1995. Phase-contrast imaging of weakly absorbing materials using hard X-rays. *Nature* **373**: 595–598.

Doube M, Kłosowski MM, Arganda-Carreras I, Cordelières FP, Dougherty RP, Jackson JS, Schmid B, Hutchinson JR, Shefelbine SJ. 2010. BoneJ: free and extensible bone image analysis in ImageJ. *Bone* **47**: 1076–1079.

Dowd BA, Campbell GH, Marr RB, Nagarkar VV, Tipnis SV, Axe L, Siddons DP. 1999. Developments in synchrotron X-ray computed microtomography at the National Synchrotron Light Source. *Proceedings of SPIE (Developments in X-Ray Tomography II)* **3772**: 224–236.

El-Sharkawy MA, Hesketh J. 1965. Photosynthesis among species in relation to characteristics of leaf anatomy and CO_2 diffusion resistances. *Crop Science* **5**: 517.

Evans JR. 2013. Improving photosynthesis. *Plant Physiology* **162**: 1780–1793.

Evans JR, Kaldenhoff R, Genty B, Terashima I. 2009. Resistances along the CO_2 diffusion pathway inside leaves. *Journal of Experimental Botany* **60**: 2235–2248.

Evans JR, von Caemmerer S, Setchell BA, Hudson GS. 1994. The relationship between CO_2 transfer conductance and leaf anatomy in transgenic tobacco with a reduced content of rubisco. *Australian Journal of Plant Physiology* **21**: 475–495.

Fujita H, Mochizuki A. 2006. The origin of the diversity of leaf venation pattern. *Developmental Dynamics* **235**: 2710–2721.

Galmés J, Ochogavía JM, Gago J, Roldán EJ, Cifre J, Conesa MÀ. 2013. Leaf responses to drought stress in Mediterranean accessions of *Solanum lycopersicum*: anatomical adaptations in relation to gas exchange parameters. *Plant, Cell & Environment* **36**: 920–935.

Giuliani R, Koteyeva N, Voznesenskaya E, Evans MA, Cousins AB, Edwards GE. 2013. Coordination of leaf photosynthesis, transpiration, and structural traits in rice and wild relatives (genus *Oryza*). *Plant Physiology* **162**: 1632–1651.

Gürsoy D, De Carlo F, Xiao X, Jacobsen C. 2014. TomoPy: a framework for the analysis of synchrotron tomographic data. *Journal of Synchrotron Radiation* **21**: 1188–1193.

Ho QT, Berghuijs HNC, Watté R, Verboven P, Herremans E, Yin X, Retta MA, Aernouts B, Saeys W, Helfen L *et al.* 2016. Three-dimensional microscale modelling of CO_2 transport and light propagation in tomato leaves enlightens photosynthesis. *Plant, Cell & Environment* **39**: 50–61.

Ivanova LA, P'yankov VI. 2002. Structural adaptation of the leaf mesophyll to shading. *Russian Journal of Plant Physiology* **49**: 419–431.

James SA, Smith WK, Vogelmann TC. 1999. Ontogenetic differences in mesophyll structure and chlorophyll distribution in *Eucalyptus globulus* ssp. *globulus*. *American Journal of Botany* **86**: 198–207.

Kittelmann M, Hawes C, Hughes L. 2016. Serial block face scanning electron microscopy and the reconstruction of plant cell membrane systems. *Journal of Microscopy-Oxford* **263**: 200–211.

Kubínová L. 1994. Recent stereological methods for measuring leaf anatomical characteristics: estimation of the number and sizes of stomata and mesophyll cells. *Journal of Experimental Botany* **45**: 119–127.

Kubínová Z, Janáček J, Lhotakova Z, Kubínová L, Albrechtová J. 2014. Unbiased estimation of chloroplast number in mesophyll cells: advantage of a genuine three-dimensional approach. *Journal of Experimental Botany* **65**: 609–620.

Lhotáková Z, Albrechtová J, Janáček J, Kubínová L. 2008. Advantages and pitfalls of using free-hand sections of frozen needles for three-dimensional analysis of mesophyll by stereology and confocal microscopy. *Journal of Microscopy* **232**: 56–63.

Longstreth DJ, Hartsock TL, Nobel PS. 1980. Mesophyll cell properties for some C_3 and C_4 species with high photosynthetic rates. *Physiologia Plantarum* **48**: 494–498.

Mandelbrot B. 1967. How long is the coast of Britain? Statistical self-similarity and fractional dimension. *Science* **156**: 636–638.

Morison JIL, Lawson T, Cornic G. 2007. Lateral CO_2 diffusion inside dicotyledonous leaves can be substantial: quantification in different light intensities. *Plant Physiology* **145**: 680–690.

Morris P, Thain JF. 1983. Improved methods for the measurement of total cell surface area in leaf mesophyll tissue. *Journal of Experimental Botany* **34**: 95–98.

Nelson EA, Sage TL, Sage RF. 2005. Functional leaf anatomy of plants with crassulacean acid metabolism. *Functional Plant Biology* **32**: 409–419.

Nobel PS. 1976. Photosynthetic rates of sun versus shade leaves of *Hyptis emoryi* Torr. *Plant Physiology* **58**: 218–223.

Nobel PS. 1977. Internal leaf area and cellular CO_2 resistance: photosynthetic implications of variations with growth conditions and plant species. *Physiologia Plantarum* **40**: 137–144.

Nobel PS, Zaragoza LJ, Smith WK. 1975. Relation between mesophyll surface area, photosynthetic rate, and illumination level during development for leaves of *Plectranthus parviflorus* Henckel. *Plant Physiology* **55**: 1067–1070.

Oi T, Enomoto S, Nakao T, Arai S, Yamane K, Taniguchi M. 2017. Three-dimensional intracellular structure of a whole rice mesophyll cell observed with FIB-SEM. *Annals of Botany*. doi: 10.1093/aob/mcx036.

Onoda Y, Wright IJ, Evans JR, Hikosaka K, Kitajima K, Niinemets Ü, Poorter H, Tosens T, Westoby M. 2017. Physiological and structural tradeoffs underlying the leaf economics spectrum. *New Phytologist* **113**: 4098.

Parkhurst DF. 1982. Stereological methods for measuring internal leaf structure variables. *American Journal of Botany* **69**: 31–39.

Parkhurst DF, Mott KA. 1990. Intercellular diffusion limits to CO_2 uptake in leaves. *Plant Physiology* **94**: 1024–1032.

Pieruschka R, Schurr U, Jensen M, Wolff WF, Jahnke S. 2006. Lateral diffusion of CO_2 from shaded to illuminated leaf parts affects photosynthesis inside homobaric leaves. *New Phytologist* **169**: 779–787.

R Core Team. 2017. *R: a language and environment for statistical computing*. Vienna, Austria: R Foundation for Statistical Computing.

Russin WA, Trivett CL. 2001. Vacuum-microwave combination for processing plant tissues for electron microscopy. In: Giberson RT, Demaree RS, eds. *Microwave techniques and protocols*. Totowa, NJ, USA: Humana Press, 25–35.

Sack L, Chatelet DS, Scoffoni C, PrometheusWiki contributors. 2013. Estimating the mesophyll surface area per leaf area from leaf cell and tissue dimensions measured from transverse cross-sections. *PrometheusWiki*. [WWW document] URL: http://prometheuswiki.org/tiki-index.php?page=Estimating+the+mesophyll+surface+area+per+leaf+area+from+leaf+cell+and+tissue+dimensions+measured+from+transverse+cross-sections [accessed 5 April 2017].

Schneider CA, Rasband WS, Eliceiri KW. 2012. NIH Image to ImageJ: 25 years of image analysis. *Nature Methods* **9**: 671–675.

Slaton MR, Smith WK. 2002. Mesophyll architecture and cell exposure to intercellular air space in alpine, desert, and forest species. *International Journal of Plant Sciences* **163**: 937–948.

Staedler YM, Masson D, Schönenberger J. 2013. Plant tissues in 3D via X-ray tomography: simple contrasting methods allow high resolution imaging. *PLoS ONE* **8**: e75295.

Talbot MJ, White RG. 2013. Methanol fixation of plant tissue for scanning electron microscopy improves preservation of tissue morphology and dimensions. *Plant methods* **9**: 36.

Terashima I, Hanba YT, Tazoe Y, Vyas P, Yano S. 2006. Irradiance and phenotype: comparative eco-development of sun and shade leaves in relation to photosynthetic CO_2 diffusion. *Journal of Experimental Botany* **57**: 343–354.

Thain JF. 1983. Curvature correction factors in the measurement of cell surface areas in plant tissues. *Journal of Experimental Botany* **34**: 87–94.

Théroux-Rancourt G, Gilbert ME. 2017. The light response of mesophyll conductance is controlled by structure across leaf profiles. *Plant, Cell & Environment* **40**: 726–740.

Tholen D, Boom C, Noguchi KO, Ueda S, Katase T, Terashima I. 2008. The chloroplast avoidance response decreases internal conductance to CO_2 diffusion in *Arabidopsis thaliana* leaves. *Plant, Cell & Environment* **31**: 1688–1700.

Tholen D, Zhu X-G. 2011. The mechanistic basis of internal conductance: a theoretical analysis of mesophyll cell photosynthesis and CO_2 diffusion. *Plant Physiology* **156**: 90–105.

Tosens T, Niinemets Ü, Vislap V, Eichelmann H, Castro Díez P. 2012. Developmental changes in mesophyll diffusion conductance and photosynthetic capacity under different light and water availabilities in *Populus tremula*: how structure constrains function. *Plant, Cell & Environment* **35**: 839–856.

Tosens T, Nishida K, Gago J, Coopman RE, Cabrera HM, Carriquí M, Laanisto L, Morales L, Nadal M, Rojas R *et al.* 2016. The photosynthetic capacity in 35 ferns and fern allies: mesophyll CO_2 diffusion as a key trait. *New Phytologist* **209**: 1576–1590.

Turrell FM. 1936. The area of the internal exposed surface of dicotyledon leaves. *American Journal of Botany* **23**: 255–264.

Uwins PJ, Murray M, Gould RJ. 1993. Effects of four different processing techniques on the microstructure of potatoes: comparison with fresh samples in the ESEM. *Microscopy Research and Technique* **25**: 412–418.

Winter H, Robinson DG, Heldt HW. 1993. Subcellular volumes and metabolite concentrations in barley leaves. *Planta* **191**: 180–190.

Wuyts N, Palauqui J-C, Conejero G, Verdeil J-L, Granier C, Massonnet C. 2010. High-contrast three-dimensional imaging of the Arabidopsis leaf enables the analysis of cell dimensions in the epidermis and mesophyll. *Plant Methods* **6**: 17.

Zhu X-G, Long SP, Ort DR. 2010. Improving photosynthetic efficiency for greater yield. *Annual Review of Plant Biology* **61**: 235–261.

Supporting Information

Additional Supporting Information may be found online in the Supporting Information tab for this article:

Table S1 Supplementary information on the plant specimens used

Methods S1 Thain (1983) curvature correction methods and accompanying R code.

Notes S1 Detailed description and background of the four S_m methods compared in this study.

Please note: Wiley Blackwell are not responsible for the content or functionality of any Supporting Information supplied by the authors. Any queries (other than missing material) should be directed to the *New Phytologist* Central Office.